J. Fluid Mech. (2001), *vol.* 447, *pp.* 337–355. © 2001 Cambridge University Press
DOI: 10.1017/S0022112001006000 Printed in the United Kingdom

A fast method for fully nonlinear water-wave computations

By DIDIER CLAMOND AND JOHN GRUE

Mechanics Division, Department of Mathematics, University of Oslo,
PO Box 1053 Blindern, 0316 Oslo, Norway
e-mail: didier@math.uio.no and johng@math.uio.no

(Received 4 July 2000 and in revised form 2 April 2001)

A fast computational method for fully nonlinear non-overturning water waves is derived in two and three dimensions. A corresponding time-stepping scheme is developed in the two-dimensional case. The essential part of the method is a fast converging iterative solution procedure of the Laplace equation. One part of the solution is obtained by fast Fourier transform, while another part is highly nonlinear and consists of integrals with kernels that decay quickly in space. The number of operations required is asymptotically $O(N \log N)$, where N is the number of nodes at the free surface. While any accuracy of the computations is achieved by a continued iteration of the equations, one iteration is found to be sufficient for practical computations, while maintaining high accuracy. The resulting explicit approximation of the scheme is tested in two versions. Simulations of nonlinear wave fields with wave slope even up to about unity compare very well with reference computations. The numerical scheme is formulated in such a way that aliasing terms are partially or completely avoided.

1. Introduction

Fully nonlinear models for water waves are employed to study various complex wave phenomena. These include the important topic of nonlinear inviscid potential flow with a free surface (recent reviews may be found in e.g. Tsai & Yue 1996 and Dias & Kharif 1999). A common drawback of the existing fully nonlinear methods, however, is that the computational schemes are slow. This means that long time simulations of wave fields with appreciable size are unrealistic. Although the integration of the prognostic equations can be made fast, the bottleneck is the solution of the Laplace equation which is required at each time step. Thus, a fully nonlinear model for water waves can only be fast provided that the Laplace equation solver is fast. Fully nonlinear and fast wave models that can be used to analyse in a realistic way highly nonlinear wave phenomena, such as freak waves, steep transient waves or steep irregular wave fields, are lacking (ISSC 2000). This is the motivation of the present study where the primary focus is to derive a fast and robust Laplace equation solver, and thereby a computationally fast model for fully nonlinear water waves.

Computationally fast fully or highly nonlinear methods exist, but they have various drawbacks that limit their usefulness. The methods by Fornberg (1980), Balk (1996) and Longuet-Higgins (2000), applying a conformal mapping, are efficient but have the disadvantage that the spatial resolution becomes poor at the crest of steep waves, where high resolution is required. Conversely, computational nodes become

dense at the troughs. Further, the methods can only be used for one-dimensional wave propagation. The high-order spectral methods outlined by Dommermuth & Yue (1987), West *et al.* (1987) and Craig & Sulem (1993) are based on Taylor series expansion about the mean water line (or about another reference level). They are computationally efficient when the series converge. For steep waves, however, the methods involve high-order derivatives and nonlinearities. The models then become numerically unstable. The gain by the added terms is lost by the necessity of stronger smoothing than for the low-order version of the method. In practice, few terms are used (Dommermuth & Yue 1987; Yasuda & Mori 1994). For highly nonlinear waves the methods do not converge. We note that slowly modulated waves may successfully be modelled by means of the nonlinear Schrödinger equation (NLS), where a narrowbanded spectrum is assumed. The modifications by Dysthe (1979) and Trulsen & Dysthe (1996) increase the bandwidth of the NLS somewhat, but the resulting equations are generally not sufficient to provide a sound model of a realistic sea.

We here derive a novel rapid method for fully nonlinear non-overturning water waves. The method is outlined for two and three dimensions. A fast Laplace equation solver is obtained by means of integral equations. One part of the solution is obtained by fast Fourier transform of the potential at the free surface and products between this potential, or its horizontal derivatives, and the wave elevation. The other part is highly nonlinear and consists of integrals that may be evaluated in a rapid way since the integrands quickly decay in space. Computations for one-dimensional wave propagation show that integration over a distance of one characteristic wavelength is sufficient for these integrals, even for highly nonlinear waves. The resulting implicit equation for the unknown function forms a basis for an iterative scheme with rapid convergence. The number of operations required is asymptotically $O(N \log N)$, where N is the number of computational nodes. Although any accuracy may be achieved by a continued iteration of the equations, one iteration is found to be sufficient for practical purposes. This forms an explicit approximation of the method which is tested in two versions. Simulations with the schemes of rather steep waves with local slope up to unity give the same results as reference computations. The computational schemes are formulated in such a way that aliasing terms are partially or completely avoided.

For simplicity, all derivations are made for water of infinite depth. The method may, however, easily be extended to variable depth. Generalizations of the method are further elaborated in the final part of the paper and in the appendices.

2. Two-dimensional motion

2.1. *Statement of the problem*

We first consider the two-dimensional problem of a fluid which is homogeneous, incompressible and inviscid. The wave-induced motion is irrotational and the depth is infinite. Let x, y and t be the horizontal, upward vertical and time variables, and let $\eta(x,t)$ be the surface elevation relative to the mean level $y = 0$. These assumptions imply the existence of a velocity potential ϕ and a stream function ψ. These quantities are linked, for $-\infty \leqslant y \leqslant \eta$, by the Cauchy–Riemann relations, $\phi_x = \psi_y$, $\phi_y = -\psi_x$. The functions ψ and ϕ_y decay to zero for $y \to -\infty$. The surface impermeability gives $\phi_y = \eta_t + \phi_x \eta_x$ at $y = \eta$. The pressure is either zero or prescribed at the surface, and the Bernoulli equation gives $g\eta + \phi_t + \frac{1}{2}\phi_x^2 + \frac{1}{2}\phi_y^2 + \tilde{p} = 0$ at $y = \eta$, where g is the acceleration due to gravity and $\tilde{p}$ the (given) pressure at the free surface. For

non-overturning waves, this set of equations can be reformulated with quantities at the surface only

$$\eta_t + \tilde{\psi}_x = 0, \quad \tilde{\phi}_t + g\eta + \frac{1}{2}\frac{\tilde{\phi}_x{}^2 - \tilde{\psi}_x^2 + 2\eta_x\tilde{\phi}_x\tilde{\psi}_x}{1+\eta_x^2} + \tilde{p} = 0, \tag{2.1}$$

where the tildes denote the functions at $y = \eta$. Other formulations are possible, involving the normal derivative of ϕ, for example. These equations are the evolution equations of η and $\tilde{\phi}$, and can be integrated once $\tilde{\psi}$ is known. The harmonic functions ϕ and ψ may be obtained in several ways. In two dimensions, the powerful theory of complex functions may be used. Using the Cauchy integral formula split into real and imaginary parts, the following equations are deduced (Baker, Meiron & Orszag 1982), in our notation

$$\tilde{\phi} = \frac{1}{\pi}\fint_{-\infty}^{\infty} \frac{D(\tilde{\phi}' - \eta_x'\tilde{\psi}') - \tilde{\psi}' - \eta_x'\tilde{\phi}'}{1+D^2}\,\frac{\mathrm{d}x'}{x'-x}, \tag{2.2}$$

$$\tilde{\psi} = \frac{1}{\pi}\fint_{-\infty}^{\infty} \frac{\tilde{\phi}' - \eta_x'\tilde{\psi}' + D(\tilde{\psi}' + \eta_x'\tilde{\phi}')}{1+D^2}\,\frac{\mathrm{d}x'}{x'-x}, \tag{2.3}$$

where $\tilde{\phi} = \tilde{\phi}(x, t)$, $\tilde{\phi}' = \tilde{\phi}(x', t)$, etc. In (2.2) and (2.3), the function $D = (\eta'-\eta)/(x'-x)$ is introduced, where D decays according to $|x'-x|^{-1}$ for $|x'-x| \to \infty$ and $D \to \eta_x$ for $x' \to x$. Equation (2.3), or equations that are similar, are commonly used to determine $\tilde{\psi}$, given $\tilde{\phi}$ and η. $\tilde{\psi}$ is then determined implicitly, and the equation is typically solved iteratively with $O(N^2)$ operations. This is the intensive part of the computations. An alternative, however, is to determine $\tilde{\psi}$ from equation (2.2). This leads to a significantly faster iterative scheme, as we shall see, than working with equation (2.3).

2.2. *Reformulation of the boundary integrals*

When the surface is horizontal, the integral equations are convolution products and can therefore be computed very quickly via a fast Fourier transform, for example. For a non-horizontal surface it is then tempting to reformulate these integrals, obtaining convolution forms. Splitting (2.2) into singular and regular integrals, we obtain after one integration by parts

$$\begin{aligned}\tilde{\phi} = &-\frac{1}{\pi}\fint_{-\infty}^{\infty}\frac{\tilde{\psi}'}{x'-x}\,\mathrm{d}x' + \frac{1}{\pi}\fint_{-\infty}^{\infty}\frac{\eta'\tilde{\phi}_x'}{x'-x}\,\mathrm{d}x' - \frac{\eta}{\pi}\fint_{-\infty}^{\infty}\frac{\tilde{\phi}_x'}{x'-x}\,\mathrm{d}x' \\ &+\frac{1}{\pi}\int_{-\infty}^{\infty}[\arctan(D) - D]\tilde{\phi}_x'\,\mathrm{d}x' + \frac{1}{\pi}\int_{-\infty}^{\infty}\frac{D(D-\eta_x')\tilde{\psi}'}{1+D^2}\,\frac{\mathrm{d}x'}{x'-x}.\end{aligned} \tag{2.4}$$

Applying the Hilbert transform, i.e.

$$\mathscr{H}\{f\} = \frac{1}{\pi}\int_{-\infty}^{\infty}\frac{f(x')}{x'-x}\,\mathrm{d}x', \quad \mathscr{H}^{-1} = -\mathscr{H},$$

equation (2.4) becomes

$$\begin{aligned}\tilde{\psi} = &\mathscr{H}\{\tilde{\phi}\} + \eta\tilde{\phi}_x + \mathscr{H}\{\eta\mathscr{H}\{\tilde{\phi}_x\}\} \\ &-\mathscr{H}\left\{\frac{1}{\pi}\int_{-\infty}^{\infty}[\arctan(D) - D]\tilde{\phi}_x'\,\mathrm{d}x' + \frac{1}{\pi}\int_{-\infty}^{\infty}\frac{D(D-\eta_x')\tilde{\psi}'}{1+D^2}\,\frac{\mathrm{d}x'}{x'-x}\right\}.\end{aligned} \tag{2.5}$$

This is another equation for $\tilde{\psi}$. In (2.5), the singular integrals are convolutions and can thus be computed quickly, with computational burden $O(N \log N)$. The remaining regular integrals have kernels that decrease rapidly, as $|x' - x|^{-3}$ and $|x' - x|^{-2}$, respectively. Therefore, integrations over $[-\infty, +\infty]$ can be approximated by integrations over a limited interval $[x - \lambda, x + \lambda]$. The parameter λ is chosen in accordance with the precision required and depends on the wave characteristics and not on the length of the computational domain (see below). Moreover, the contribution on the right-hand side of (2.5) involving $\tilde{\psi}$, is cubic in nonlinearity, whereas in equation (2.3) the corresponding term is quadratic. For non-breaking waves, where cubic terms are smaller than quadratic terms, iterations with (2.5) converge faster than iterations with (2.3).

For time-dependent simulations, the evaluation of $\tilde{\psi}$ is not needed, only $\tilde{\psi}_x$ is required. It is thus preferable to compute $\tilde{\psi}_x$ directly. One differentiation and one integration by parts of (2.5) yield

$$\tilde{\psi}_x = \mathscr{H}\{\tilde{\phi}_x\} + \partial_x\{\eta\tilde{\phi}_x\} + \partial_x\{\mathscr{H}\{\eta\mathscr{H}\{\tilde{\phi}_x\}\}\} + \mathscr{H}\left\{\frac{1}{\pi}\int_{-\infty}^{\infty} \frac{D^2(D-\eta_x)\tilde{\phi}'_x}{1+D^2}\frac{\mathrm{d}x'}{x'-x} - \frac{1}{\pi}\int_{-\infty}^{\infty} \frac{D(D-\eta_x)\tilde{\psi}'_x}{1+D^2}\frac{\mathrm{d}x'}{x'-x}\right\}. \quad (2.6)$$

An interesting feature of (2.6), is that its regular integrals involve η_x and not η'_x. For x close to a crest or a trough, η_x is close to zero. The kernels of the integrals in (2.6) then decay as $|x' - x|^{-4}$ and $|x' - x|^{-3}$, respectively. This means that a truncated integration is more efficient and accurate around crests and troughs than elsewhere. This is in contrast with Taylor expansions and methods based on conformal mapping which are poorer at wave crests.

2.3. *Remarks*

The rapid decay of the kernels is an essential reason for the efficiency of this formulation. It is not the only one, however, as can be understood by also considering the nonlinearities. For illustration we note that

$$\lim_{x'\to x} \frac{D}{1+D^2}\frac{D-\eta_x}{x'-x} = \frac{1}{2}\frac{\eta_x\eta_{xx}}{1+\eta_x^2}.$$

Since we are considering water waves, the quantities involved are functions that oscillate around zero. For deep water waves, η_x and η_{xx} are generally out of phase, meaning that the product $\eta_x\eta_{xx}$ is small. In shallow water, however, both η_x and η_{xx} may have large values at the same points. An example is the exponential decay of a large solitary wave. In this case, integrals with faster decaying kernels may be required for obtaining computationally efficient formulae. Such formulae can be obtained by the method described in Appendix A, for example. During our numerical experimentations at infinite depth, we never found the necessity to use such improved formulae, however.

Analogue transformations of (2.3), i.e. in a way that the kernels of the regular integrals decrease at least as $|x' - x|^{-2}$, give

$$\tilde{\psi} = \mathscr{H}\{\tilde{\phi}\} + \mathscr{H}\{\eta\tilde{\psi}_x\} - \eta\mathscr{H}\{\tilde{\psi}_x\} + \frac{1}{\pi}\int_{-\infty}^{\infty} \frac{D(D-\eta'_x)\tilde{\phi}'}{1+D^2}\frac{\mathrm{d}x'}{x'-x} + \frac{1}{\pi}\int_{-\infty}^{\infty} [\arctan(D) - D]\tilde{\psi}'_x\mathrm{d}x'. \quad (2.7)$$

For this equation, of the form $\tilde{\psi} = F(\tilde{\psi}_x)$, a functional iteration (see below) is

numerically unstable. This is in contrast to equation (2.6) which is of the form $\tilde{\psi}_x = F(\tilde{\psi}_x)$ and is stable. However, equation (2.7) can be applied to obtain $\tilde{\phi}$ when η and $\tilde{\psi}$ are given.

Higher nonlinear terms in $\tilde{\psi}$ can be extracted from the regular integral and written as convolutions, the remaining regular integrals having faster decreasing kernels. However, these extra convolutions involve higher derivatives and are thus not suitable for numerical computations. Similarly, the equation for ψ can be rewritten in a form involving hyper-singular integrals, with faster decaying kernels. The practical determination of these integrals requires the evaluation of the derivatives of $\tilde{\psi}$, and thus these formulae are not suitable either.

We note that Ceniceros & Hou (1998), studying interfacial flows with surface tension in two dimensions, also split their integral equation into a part with a Hilbert transform and a remainder. Whereas their focus is to prove convergence of a reformulated boundary-integral method, the important point here is to invert the appropriate equation by applying Hilbert transforms. (In the three-dimensional case, we invert the relevant equation using a Fourier transform.) This provides a better platform for analysis and computations than using the classical formulation (2.3).

3. Successive approximations

An iterative scheme for the solution of (2.6) is initialized by the explicit quadratic approximation

$$\tilde{\psi}_{2,x} = \mathscr{H}\{\tilde{\phi}_x\} + \partial_x\{\eta\tilde{\phi}_x\} + \mathscr{H}\partial_x\{\eta\mathscr{H}\{\tilde{\phi}_x\}\}. \tag{3.1}$$

Applying one analytical iteration, keeping terms up to cubic nonlinearity, we obtain an explicit cubic approximation, i.e.

$$\tilde{\psi}_{3,x,\lambda} = \tilde{\psi}_{2,x} - \mathscr{H}\left\{\frac{1}{\pi}\int_{x-\lambda}^{x+\lambda}\frac{D(D-\eta_x)}{x'-x}\mathscr{H}\{\tilde{\phi}'_x\}\,\mathrm{d}x'\right\}. \tag{3.2}$$

If terms up to quartic nonlinearity are included, we obtain the following approximation

$$\tilde{\psi}_{4,x,\lambda} = \tilde{\psi}_{2,x} - \mathscr{H}\left\{\frac{1}{\pi}\int_{x-\lambda}^{x+\lambda}\frac{D(D-\eta_x)}{1+D^2}(\tilde{\psi}'_{2,x} - D\tilde{\phi}'_x)\frac{\mathrm{d}x'}{x'-x}\right\}. \tag{3.3}$$

(Some simulations have shown that it is important to keep the denominator $1+D^2$ in the integral of (3.3) in order to obtain the desired accuracy, although this is formally beyond quartic nonlinearity.)

Considerations on further successive approximations of equation (2.6) are presented in § 3.3. At this point, we recall the primary focus of the investigation, namely the search for rapid fully nonlinear water-wave simulations for moderately steep waves, i.e. waves with $|\eta_x| < 1$, say. Keeping this in mind, we aim to test the explicit solutions (3.2)–(3.3) of the Laplace equation. All simulations presented here indicate that (3.2) predicts nonlinear wave evolution with very high accuracy when η_x is less than about 0.5. The solution of the Laplace equation given by (3.2) is very rapid and suitable for de-aliased simulations. In regions with larger values of η_x, say up to unity, we find that (3.3) provides excellent predictions of the wave field, while (3.2) then becomes somewhat inaccurate. Although (3.3) is computationally somewhat more involved than (3.2), it is still explicit, relatively rapid and provides a basis for partially de-aliased computations.

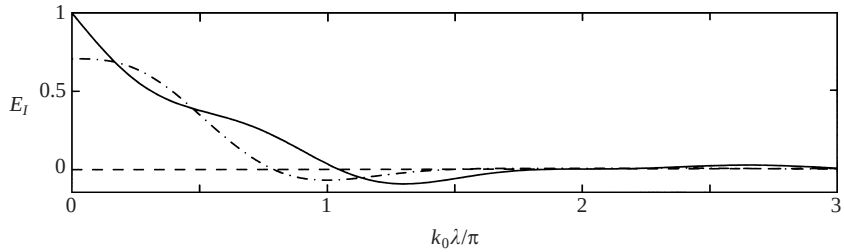

FIGURE 1. Error variation of the truncated integration (equation (3.5)). - - -, $k_0x = 0$; $-\cdot-$, $k_0x = \pi/4$; —— $k_0x = \pi/2$.

3.1. *Truncated integration*

We shall also find it sufficient to truncate the regular integrals in (3.2)–(3.3). Consider

$$I(x;\lambda) = \mathscr{H}\left\{\frac{1}{\pi}\int_{x-\lambda}^{x+\lambda}\frac{D(D-\eta_x)}{x'-x}\mathscr{H}\{\tilde{\phi}'_x\}\,\mathrm{d}x'\right\}. \tag{3.4}$$

The effect of truncation may be estimated by applying the linear approximation of a steady wave, i.e. $\eta_x \simeq -\epsilon\sin k_0x$, $\tilde{\phi}_x \simeq \epsilon c\cos k_0x$, $\tilde{\psi}_x \simeq -\epsilon c\sin k_0x$, $c^2 \simeq g/k_0$ and $\epsilon = ak_0$, giving $I(x;\infty) \simeq \frac{1}{4}\epsilon^3 c\sin(k_0x)$ and

$$\begin{aligned} E_I(x;\lambda) &\equiv \frac{I(x;\infty)-I(x;\lambda)}{\max(|I(x;\infty)|)} \\ &\sim \frac{4\sin k_0\lambda - 2\sin 2k_0\lambda}{\pi(k_0\lambda)^2}\cos 2k_0x\sin k_0x + O(\epsilon) \quad \text{as} \quad \lambda\to\infty. \end{aligned} \tag{3.5}$$

This shows that the integral decays according to $1/(k_0\lambda)^2$, to leading order in wave slope. A further analysis, based on higher Stokes approximations, will (probably) show a decay of E_I as $1/(k_0\lambda)$, but proportional (at least) to ϵ. The amplitude of $E_I(x;\lambda)$ is visualized in figure 1. We observe that about 90% of the contribution to the integral is obtained with an integration over one wavelength, i.e. $\lambda = \pi/k_0$, and 98% for two wavelengths. The effect of a truncated integration is further discussed in connection with the computations presented in § 5.

3.2. *Computational remarks*

The evaluation of the regular integral in (3.2)–(3.3) requires $O(M\times N)$ operations, where M is given by the characteristic wavelength and N by the length of the domain. This means that the total number of operations, for the calculus of (3.2)–(3.3), is $O(N\log N, NM) \sim O(N\log N)$ for $N\to\infty$.

If more precision is required, the full equation (2.6) has to be solved. Starting iterations with $\tilde{\psi}_{2,x}$ and a given λ (increased at each iteration), we therefore have a fast Laplace equation solver. For long tank simulations the number of operations remains asymptotically $O(N\log N)$.

We also remark that, with $\lambda\to\infty$, the approximated formula (3.2) can be expressed in terms of convolutions only, i.e.

$$\begin{aligned} \tilde{\psi}_{3,x} = {}& \mathscr{H}\{\tilde{\phi}_x\} + \partial_x\{\eta\tilde{\phi}_x\} + \mathscr{H}\partial_x\{\eta\mathscr{H}\{\tilde{\phi}_x\}\} \\ & + \tfrac{1}{2}\mathscr{H}\partial_x\{\eta^2\partial_x\{\tilde{\phi}_x\}\} + \mathscr{H}\partial_x\{\eta\mathscr{H}\partial_x\{\eta\mathscr{H}\{\tilde{\phi}_x\}\}\} + \tfrac{1}{2}\partial_x^2\{\eta^2\mathscr{H}\{\tilde{\phi}_x\}\}. \end{aligned} \tag{3.6}$$

Although $\tilde{\psi}_{3,x}$ and $\tilde{\psi}_{3,x,\infty}$ are equivalent analytically, the former, involving higher-order

derivatives, is numerically more unstable than the latter. $\tilde{\psi}_{3,x}$ is therefore less suitable for practical computations than $\tilde{\psi}_{3,x,\lambda}$.

3.3. *Rate of convergence of the functional iteration*

The successive approximations of the full solution of (2.6) may be continued beyond (3.1)–(3.3). For a convenient notation we introduce the linear operator $\mathscr{J}$ acting on any function f by

$$\mathscr{J}\{f\} = -\mathscr{H}\left\{\frac{1}{\pi}\int_{-\infty}^{\infty}\frac{D(D-\eta_x)f'}{1+D^2}\frac{\mathrm{d}x'}{x'-x}\right\}, \tag{3.7}$$

and introduce $Q_{n+1} = Q_n + \mathscr{J}\{Q_n\}$ $(n = 0, 1, \ldots)$, with

$$Q_0 = \mathscr{H}\{\tilde{\phi}_x\} + \partial_x(\eta\tilde{\phi}_x + \mathscr{H}\{\eta\mathscr{H}\{\tilde{\phi}_x\}\}) + \mathscr{H}\left\{\frac{1}{\pi}\int_{-\infty}^{\infty}\frac{D^2(D-\eta_x)\tilde{\phi}'_x}{1+D^2}\frac{\mathrm{d}x'}{x'-x}\right\}. \tag{3.8}$$

Successive approximations of (2.6) are then obtained by

$$\tilde{\psi}_x = Q_0 + \mathscr{J}\{\tilde{\psi}_x\} = Q_1 + \mathscr{J}^2\{\tilde{\psi}_x\} = \cdots = Q_n + \mathscr{J}^{n+1}\{\tilde{\psi}_x\} = \cdots, \tag{3.9}$$

where $\mathscr{J}^2\{f\} = \mathscr{J}\{\mathscr{J}\{f\}\}$, etc. The error of the nth approximation is given by

$$e_n = \tilde{\psi}_x - Q_n = \mathscr{J}^{n+1}\{\tilde{\psi}_x\} = \mathscr{J}\{e_{n-1}\}. \tag{3.10}$$

The rate of convergence of the iteration procedure is indicated by the ratio $|e_{n+1}/e_n|$ and may be estimated from the linear approximation of a steady wave, giving

$$\mathscr{J}\{\tilde{\psi}_x\} = -\tfrac{1}{4}\epsilon^3 c\sin(k_0 x) + O(\epsilon^4). \tag{3.11}$$

This means that $|e_{n+1}/e_n| = \epsilon^2/4$ to leading order in the wave slope, indicating rapid convergence of the method. This result could be anticipated since $\mathscr{J}$ is cubic in nonlinearity.

A corresponding estimate for equation (2.7) is $|e_{n+1}/e_n| = 3\epsilon/2$, indicating a slower convergence of a functional iteration in this case. We have found that this procedure for (2.7) is numerically unstable, however, as already mentioned in § 2.3.

4. Implementation of unsteady numerical simulations

The fast Cauchy solver is one part of the numerics required for the simulation of water waves. A method for solving the prognostic equations is demonstrated here.

4.1. *Temporal scheme*

The original system of equations (2.1) may be put into conservative form involving dimensionless dependent variables. Applying one differentiation with respect of x, one Fourier transform, and separating the linear and nonlinear parts, it can be rewritten into a more suitable system

$$\begin{bmatrix} \partial_t & -\omega \\ \omega & \partial_t \end{bmatrix}\begin{pmatrix} \mathscr{F}\{\eta_x\} \\ \dfrac{\omega}{g}\mathscr{F}\{\tilde{\phi}_x\} \end{pmatrix} + \begin{pmatrix} 0 \\ \dfrac{\omega}{g}\mathscr{F}\{\tilde{p}_x\} \end{pmatrix} = -\mathrm{i}k\begin{pmatrix} \mathscr{F}\{\tilde{\psi}_x - \mathscr{H}\{\tilde{\phi}_x\}\} \\ \dfrac{\omega}{g}\mathscr{F}\left\{\dfrac{\tilde{\phi}_x{}^2 - \tilde{\psi}_x^2 + 2\eta_x\tilde{\phi}_x\tilde{\psi}_x}{2(1+\eta_x^2)}\right\} \end{pmatrix}, \tag{4.1}$$

where $\omega^2 = g|k|$ and $\mathscr{F}$ denotes the Fourier transform (i.e. $\mathscr{F}\{f\}(k) = \int_{-\infty}^{\infty} f(x)\,\mathrm{e}^{-\mathrm{i}kx}\mathrm{d}x$). The linear part of (4.1) is integrated analytically, while the nonlinear part is solved numerically with a variable step-size eighth-order explicit Runge–Kutta scheme (Hairer,

Nørsett & Wanner 1987). The scheme is therefore unconditionally (linearily) stable and accurate. This high-order scheme provides relatively large time steps and is thus a fast scheme with little accumulation of round-off error.

The spatial derivatives are computed in the Fourier space and the nonlinear terms are calculated in the physical space. Both the Fourier and physical spaces are periodic and discretized with a constant step.

4.2. *Fully and partially 'de-aliased' computations*

Several authors – Longuet-Higgins & Cokelet (1976), Dommermuth & Yue (1987), Craig & Sulem (1993), among others – have observed the so-called *sawtooth instabilities* in their numerical models. This important problem has been circumvented using smoothing. For example, Craig & Sulem, following Dommermuth & Yue, used a five-point moving average which is equivalent to a low-pass filter in Fourier space. This method indeed damps the highest wavenumbers, but also the lower ones. This is therefore not suitable for long-time simulations, since the energy of a wave field decreases in time, and eventually vanishes. These sawtooth instabilities are due to aliasing and, instead of smoothing, we employ the following method to prevent them.

Products of discrete functions in physical space are circular convolutions in Fourier space (i.e. the spectra are periodic). De-aliased computations can be performed by extending the spectra by zeros padding (Canuto *et al.* 1987, Chap. 3). The spectra must (at least) be extended by a factor of $3/2$ for quadratic nonlinearities, and by a factor of $4/2$ for cubic nonlinearities, etc. Water-wave equations involve non-polynomial nonlinearities such as $(1+\eta_x^2)^{-1}$, on the other hand. This kind of nonlinearity does not reduce to a finite number of convolutions in Fourier space. Therefore, whatever the length of the zeros padding, the entire spectrum is polluted by aliasing if these terms are computed directly.

If $\tilde{\psi}_x$ is computed with the cubic approximation (3.2), the calculus becomes fully de-aliased by doubling the spectra (4-halves rule). For the temporal simulations, fully de-aliased computations can hence be carried out using the 4-halves rule, setting to zero the extra wavenumbers each time a cubic nonlinearity is computed. The non-polynomial nonlinearity of the Bernoulli equation can be computed, without aliasing, via some accurate polynomial approximations, such as Taylor expansions, Chebychev polynomials, etc. As a simple illustration of the method, we can: (i) compute $\tilde{\phi}_x^2 - \tilde{\psi}_x^2 + 2\eta_x\tilde{\phi}_x\tilde{\psi}_x$ and η_x^3; (ii) set to zero the extra wavenumbers of these quantities; (iii) compute

$$\frac{\tilde{\phi}_x{}^2 - \tilde{\psi}_x^2 + 2\eta_x\tilde{\phi}_x\tilde{\psi}_x}{1+\eta_x^2} \simeq [\tilde{\phi}_x{}^2 - \tilde{\psi}_x^2 + 2\eta_x\tilde{\phi}_x\tilde{\psi}_x] \times [1 - \eta_x \times \eta_x + \eta_x \times \eta_x^3 - \eta_x^3 \times \eta_x^3]; \quad (4.2)$$

(iv) set to zero the extra wavenumbers of the quantity (4.2). The relative error of (4.2) is less than 0.4% for $\eta_x = 0.5$. Many other polynomial approximations can be employed. If more precision is required, higher-order polynomials must be used, but the principle of the method remains the same.

If $\tilde{\psi}_x$ is computed with the (almost) quartic approximation (3.3), the calculus cannot be fully de-aliased (at a reasonable cost). However, partially de-aliased computations can be achieved using the 4-halves rule and setting to zero the extra wavenumbers each time an almost cubic nonlinearity is computed. For example, to compute the nonlinear term of the Bernoulli equation, we can: (i) compute $A = \tilde{\phi}_x^2 - \tilde{\psi}_x^2 + 2\eta_x\tilde{\phi}_x\tilde{\psi}_x$ and $B = 1 + \eta_x^2$; (ii) set to zero the extra wavenumbers of A and B; (iii) compute A/B; (iv) set to zero the extra wavenumbers of the latter. This method is efficient while the error due to aliasing is comparable to that due to round-off.

Formulae giving $\tilde{\psi}_x$	Computational Nodes Per Wavelength			
	$8+8$	$16+16$	$32+32$	$64+64$
$\tilde{\psi}_{2,x}$	1.47	1.47	1.47	1.47
$\tilde{\psi}_{3,x,\pi/k_0}$	0.24	0.15	0.15	0.15
$\tilde{\psi}_{4,x,\pi/k_0}$	0.20	0.10	0.11	0.11
$\tilde{\psi}_{x,\text{classical}}$	2.29	0.02	0.00	0.00
$\tilde{\psi}_{2,x}$	6.89	4.70	4.86	4.86
$\tilde{\psi}_{3,x,\pi/k_0}$	4.52	0.63	0.32	0.32
$\tilde{\psi}_{4,x,\pi/k_0}$	4.56	0.56	0.25	0.26
$\tilde{\psi}_{x,\text{classical}}$	16.4	1.68	0.03	0.03

TABLE 1. Relative maximal error (%) between reference and approximated $\tilde{\psi}_x$, for steady Stokes waves, with $ak_0 = 0.21$ (upper) and $ak_0 = 0.35$ (lower).

The same partial de-aliasing method can be used when $\tilde{\psi}_x$ is given by the classical formula (2.3). However, for periodic domains (see Appendix C, equation (C 1)), the latter involves transcendental functions and requires numerical iterations. The resulting $\tilde{\psi}_x$ is therefore much more aliased. This is another argument in favour of the formulae derived from (2.6).

The anti-aliasing procedure preserves the spectra and can be viewed, instead of smoothing, as a 'radiation condition' in Fourier space. With this method, no smoothing or regridding appeared to be necessary during our numerical experimentations.

5. Numerical examples

5.1. *Comparisons with an exact steady solution*

We first compare our formulae with an exact solution of Stokes waves (Fenton 1988). Using his program with 16 Fourier nodes, we obtain reference values of η, $\tilde{\phi}_x$ and $\tilde{\psi}_x$ for $ak_0 = 0.21$ and $ak_0 = 0.35$ (a denotes the wave amplitude and k_0 the wavenumber). We then obtain $\tilde{\psi}_x$ from (3.1)–(3.3) and (C 1) (the periodic version of (2.3), given in Appendix C). Each computation is achieved applying the 4-halves rule. The relative maximal deviation of the approximated $\tilde{\psi}_x$ from the reference, i.e. the ∞-norm, is then evaluated. The results in table 1 illustrate that $\tilde{\psi}_{3,x,\pi/k_0}$ and $\tilde{\psi}_{4,x,\pi/k_0}$ provide excellent approximations to the function. Both $\tilde{\psi}_{3,x,\pi/k_0}$ and $\tilde{\psi}_{4,x,\pi/k_0}$ are closer to the reference function than $\tilde{\psi}_x$ obtained by the ordinary formulation (2.3) when the grids are coarse, more specifically for $8+8$ computational nodes per wavelength when $ak_0 = 0.21$ and $16+16$ nodes when $ak_0 = 0.35$. This illustrates the effect of aliasing on the computations. The feature that the explicit approximations gain high accuracy with coarse grids can advantageously be exploited in simulations of long wave fields. The classical formulation converges to the reference solution for high resolution of the wave field, as could be anticipated. The approximation $\tilde{\psi}_{2,x}$ is relevant only for small ak_0.

5.2. *Wave generation*

We also simulate waves generated by a pneumatic wavemaker starting from rest, comparing schemes using (2.3) and (3.2). We consider the generation of a monochromatic wave – of wavenumber k_0 and amplitude a – by a varying pressure with a Gaussian

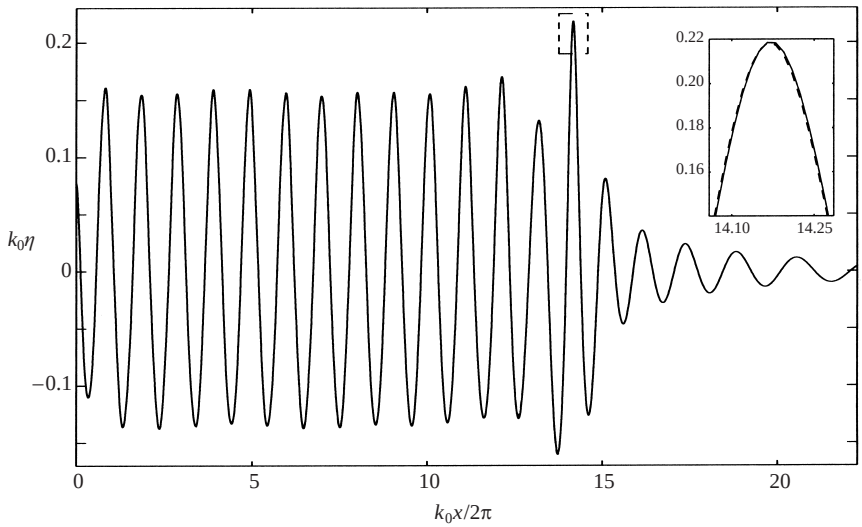

FIGURE 2. The transient leading part of a wave train. Pneumatic wave generation. —, $\tilde{\psi}_{x,\text{classical}}$; – –, $\tilde{\psi}_{3,x,\pi/k_0}$.

spatial distribution. For $t < 0$, $\tilde{p}$ is zero, while, for $t \geqslant 0$, we consider

$$\frac{\omega}{g}\mathscr{F}\{\tilde{p}_x\} = a\sqrt{gk_0}\exp\left(\frac{k_0^2 - k^2}{2k_0^2}\right)\left(\frac{k}{k_0}\right)^{3/2}\sin(\sqrt{gk_0}t). \tag{5.1}$$

This pneumatic wavemaker has been tuned in order to transmit a maximal energy to the wave in the far field (Wehausen & Laitone 1960, § 21). More details on this simulation can be found in Clamond & Grue (2000).

The results show that the two methods are almost identical, where the differences, measured by the root mean square, are less than 1% (figure 2). The use of $\tilde{\psi}_{3,x,\pi/k_0}$ gave the results about fifteen times faster than by using equation (2.3), for a computational domain of about thirty characteristic wavelengths. If a longer tank is used, the gain increases. We note that the wave broke a few time steps later than the profile shown in figure 2. This illustrates the high nonlinearity of the unsteady steep wave. (Similar wave breaking is also observed in a physical wave tank.)

5.3. *Wave–wave interaction*

Modulated periodic waves are now simulated comparing $\tilde{\psi}_{3,x,\pi/k_0}$, $\tilde{\psi}_{4,x,\pi/k_0}$ and $\tilde{\psi}_x$ obtained by (C 1). Recent works on this subject (Dold & Peregrine 1986; Banner & Tian 1998) find that either rapid onset of wave breaking or recurrence of the initial state takes place depending on the magnitude of the initial wave slope. Our initial wave field is similar to those studied by these authors, except that the wave slope is selected somewhat larger, stimulating more rapid growth of the instabilities. Convergence of the reference computations is then more certain than for weak nonlinearity, where a simulation over long time is required.

The surface elevation of an exact Stokes waves, with initial wave slope $ak_0 = 0.22$ and extended in a periodic wave tank being 8 wavelengths long, is perturbed by

$$\varepsilon a\cos\left(\frac{n+m}{n}k_0x - \frac{\pi}{4}\right) + \varepsilon a\cos\left(\frac{n-m}{n}k_0x - \frac{\pi}{4}\right), \tag{5.2}$$

where in the simulations $n = 8$, $m = 1$ and $\varepsilon = 0.105$. A corresponding perturbation

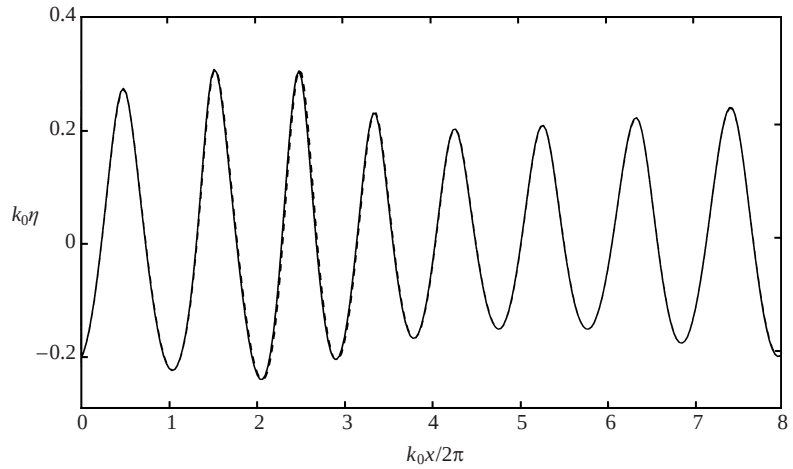

FIGURE 3. Wave–wave interaction after 16 periods. Initial train: Stokes wave + sinusoidal perturbation. ——, $\tilde{\psi}_{x,\text{classical}}$; — —, $\tilde{\psi}_{3,x,\pi/k_0}$.

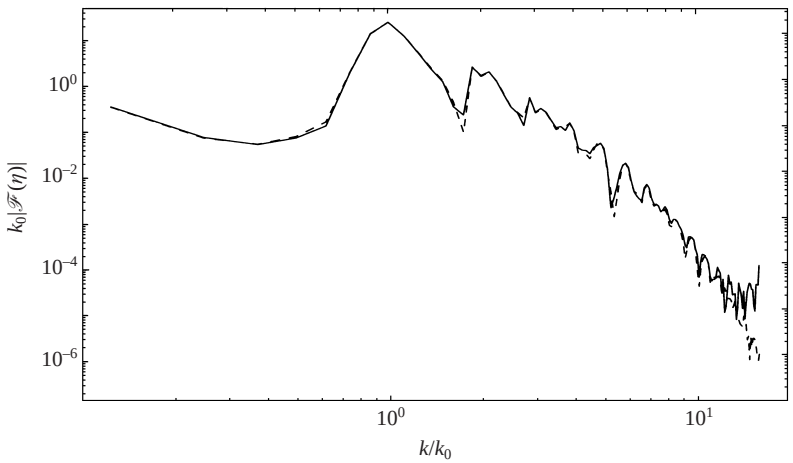

FIGURE 4. Spectrum after 16 periods. ——, $\tilde{\psi}_{x,\text{classical}}$; — —, $\tilde{\psi}_{3,x,\pi/k_0}$.

is used for the velocity field (see Dold & Peregrine 1986 or Banner & Tian 1998 for further details about this simulation). The number of computational nodes per wavelength is $32 + 32$ (which means that wavenumber up to the 15th harmonic is resolved).

The instabilities grow in time. After 16 wave periods the maximal wave slope $|\eta_x|$ has become 0.344 (figure 3). Simulations of the wave field using $\tilde{\psi}_{3,x,\pi/k_0}$ compare favourably with the classical formulation (C 1). The spectrum $\mathscr{F}\{\eta\}$ of the surface elevation further demonstrate the excellent correspondence between the two schemes (figure 4). The good comparison of the spectrum illustrates that the two schemes both capture the physical nonlinear development of the wavetrain. We note that the solution with (C 1) exhibits weak aliasing errors for very high wavenumbers. This effect is absent for the de-aliased simulations with $\tilde{\psi}_{3,x,\pi/k_0}$, however.

The instabilities of the wave field continues to grow. Predictions of the wave profile

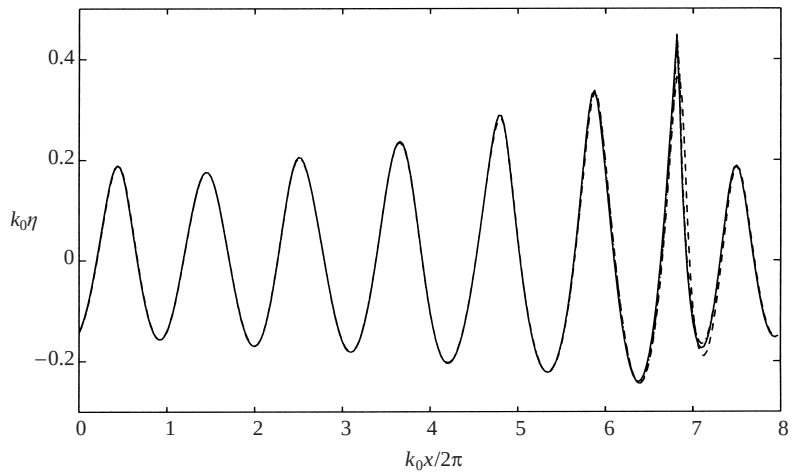

FIGURE 5. Wave–wave interaction after 23 periods. ——, $\tilde{\psi}_{x,\text{classical}}$; — —, $\tilde{\psi}_{3,x,\pi/k_0}$; – · –, $\tilde{\psi}_{4,x,\pi/k_0}$.

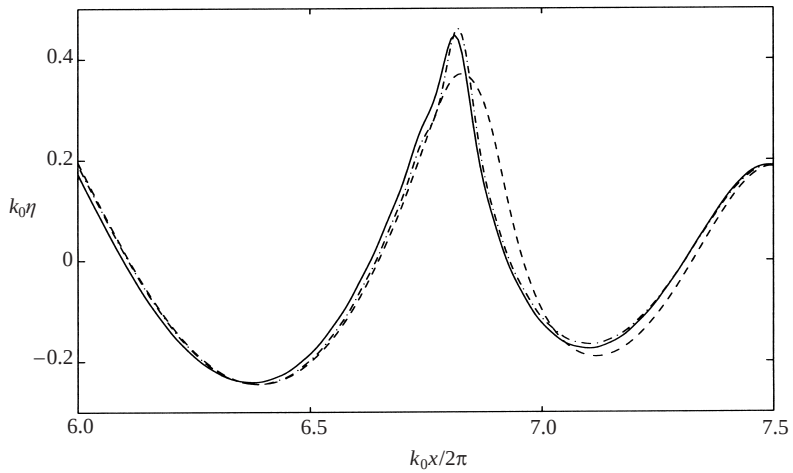

FIGURE 6. Same as figure 5. ——, $\tilde{\psi}_{x,\text{classical}}$; — —, $\tilde{\psi}_{3,x,\pi/k_0}$, – · –, $\tilde{\psi}_{4,x,\pi/k_0}$.

using $\tilde{\psi}_{3,x,\pi/k_0}$, $\tilde{\psi}_{4,x,\pi/k_0}$ are visualized in figures 5 and 6 after 23 wave periods. Now the maximal value of $|\eta_x|$ has increased to 0.87. While $\tilde{\psi}_{4,x,\pi/k_0}$ and $\tilde{\psi}_x$ obtained by (C 1) compare well for the whole wave field, $\tilde{\psi}_{3,x,\pi/k_0}$ shows an overall favourable agreement, but is less good at the largest wave, however. We also evaluate the spectrum of the surface elevation. This shows a pronounced transfer of energy from moderate to high wavenumbers. The spectrum shows an almost perfect agreement between $\tilde{\psi}_{4,x,\pi/k_0}$ and $\tilde{\psi}_x$ obtained by (C 1) (figure 7). The spectrum of $\tilde{\psi}_{3,x,\pi/k_0}$ compares well with the more full schemes, for intermediate wavenumbers, but does not capture the energy transfer to short wave modes satisfactorily. We further note that some deviation for rather low wavenumbers also takes place. It is evident from the spectra that the computations with $\tilde{\psi}_{4,x,\pi/k_0}$ and $\tilde{\psi}_x$ from (C 1) capture the physical development in the wave–wave interactions of the wave field. The rather strong transfer of energy from moderate to large wavenumbers hides the (small) aliasing errors in the computations using $\tilde{\psi}_{4,x,\pi/k_0}$ and the classical $\tilde{\psi}_x$ (the schemes of the latter are not fully de-aliased).

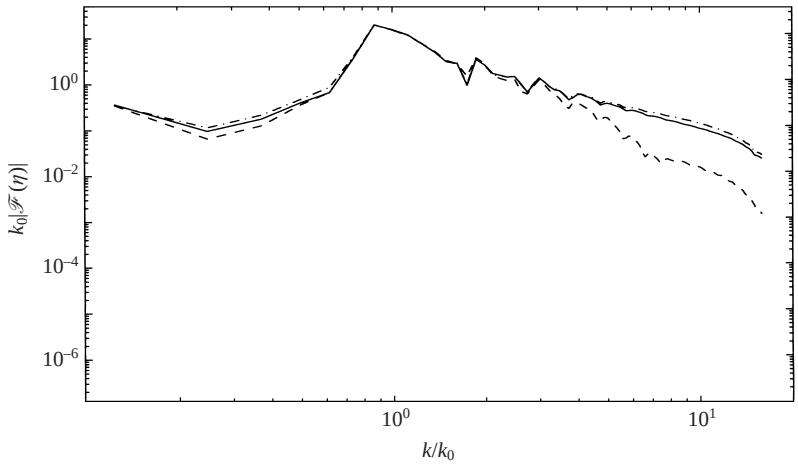

FIGURE 7. Spectrum after 23 periods. ——, $\tilde{\psi}_{x,\text{classical}}$; – –, $\tilde{\psi}_{3,x,\pi/k_0}$; –·–, $\tilde{\psi}_{4,x,\pi/k_0}$.

We note that the use of the formulae for $\tilde{\psi}_{3,x,\pi/k_0}$ and $\tilde{\psi}_{4,x,\pi/k_0}$ speed up the time simulations by a factor of about hundred in these examples as compared to the classical procedure. This is logical since, for such steep waves, the classical formula requires many iterations. The computing time using $\tilde{\psi}_{3,x,\pi/k_0}$ is about 20% less than using $\tilde{\psi}_{4,x,\pi/k_0}$. We further note that there is not much difference in computing time taking into account the denominator $1+D^2$ in the formulae. An important difference is that computations with $\tilde{\psi}_{3,x,\pi/k_0}$ may be completely de-aliased.

The simulations here indicate that we may use $\tilde{\psi}_{3,x,\pi/k_0}$ when $\max|\eta_x|$ is less than around 0.35, and $\tilde{\psi}_{4,x,\pi/k_0}$ when $\max|\eta_x|$ is in the interval 0.35–0.9. We note that it is not certain that the computations achieved with the classical $\tilde{\psi}_x$ are better than those using $\tilde{\psi}_{4,x,\pi/k_0}$, since the former induces more aliasing error.

6. Generalization to three dimensions

Generalization to three dimensions is then considered. In this case the Laplace equation has to be solved in a way other than by using complex theory, since the latter is limited to two-dimensional flows. Green's theorem is applied for this purpose. The y-coordinate is kept as above, while $\boldsymbol{x} = (x_1, x_2)$ are the two horizontal Cartesian coordinates.

The prognostic equations in three dimensions are similar to those in the two-dimensional case as given in equation (2.1) (see Tsai & Yue 1996). These equations update the velocity potential $\tilde{\phi}$ at the free surface and the elevation η when the (outgoing) normal velocity ϕ_n is known. The latter is obtained from the solution of the Laplace equation when $\tilde{\phi}$ and η are given on the free surface. As in the previous paragraphs we assume that the depth of the water is infinite. From Green's theorem we have

$$\iint_S \frac{1}{r}\frac{\partial \phi'}{\partial n'}\,\mathrm{d}S = 2\pi\tilde{\phi} + \iint_S \tilde{\phi}'\frac{\partial}{\partial n'}\frac{1}{r}\,\mathrm{d}S, \tag{6.1}$$

where $\tilde{\phi} = \tilde{\phi}(\boldsymbol{x})$, $\tilde{\phi}' = \tilde{\phi}(\boldsymbol{x}')$, $r = [\boldsymbol{R}^2 + (y'-y)^2]^{1/2}$, $\boldsymbol{R} = (\boldsymbol{x}' - \boldsymbol{x})$ and S denotes the free surface. The element of the latter is given by $\mathrm{d}S = \sqrt{1+(\nabla'\eta')^2}\,\mathrm{d}\boldsymbol{x}'$, where $\nabla = (\partial_{x_1}, \partial_{x_2})$ denotes the horizontal gradient and $\mathrm{d}\boldsymbol{x} = \mathrm{d}x_1\mathrm{d}x_2$ is the element of

horizontal surface, giving

$$\iint_{-\infty}^{\infty} \frac{V'}{(1+D^2)^{1/2}} \frac{\mathrm{d}\boldsymbol{x}'}{R} = 2\pi\tilde{\phi} + \iint_{-\infty}^{\infty} \frac{\tilde{\phi}'}{(1+D^2)^{3/2}} \left(\frac{\boldsymbol{R}\cdot\nabla'\eta'}{R^3} - \frac{\eta'-\eta}{R^3} \right) \mathrm{d}\boldsymbol{x}', \tag{6.2}$$

where $R^2 = \boldsymbol{R}\cdot\boldsymbol{R}$, $V = \phi_n\sqrt{1+(\nabla\eta)^2}$ and $D = (\eta'-\eta)/R$ are introduced. We have $D \sim R^{-1}$ for $R \to \infty$ and $D \to \eta_R$ for $R \to 0$. We now exploit

$$\frac{\boldsymbol{R}\cdot\nabla'\eta'}{R^3} - \frac{\eta'-\eta}{R^3} = -\nabla'\cdot\left[(\eta'-\eta)\nabla'\frac{1}{R}\right]. \tag{6.3}$$

By application of the Gauss theorem we may partially rewrite the last term in (6.2). The modified and reorganized version of the equation reads

$$\iint_{-\infty}^{\infty} \frac{V'}{R}\,\mathrm{d}\boldsymbol{x}' = 2\pi\tilde{\phi} + \iint_{-\infty}^{\infty} (\eta'-\eta)\nabla'\tilde{\phi}'\cdot\nabla'\frac{1}{R}\,\mathrm{d}\boldsymbol{x}' - \iint_{-\infty}^{\infty} \frac{V'}{R}[(1+D^2)^{-1/2}-1]\,\mathrm{d}\boldsymbol{x}'$$
$$- \iint_{-\infty}^{\infty} \tilde{\phi}'[(1+D^2)^{-3/2}-1]\nabla'\cdot\left[(\eta'-\eta)\nabla'\frac{1}{R}\right]\mathrm{d}\boldsymbol{x}'. \tag{6.4}$$

A decomposition $V = V_1 + V_2 + V_3 + V_4$ is then introduced, where V_1, V_2, V_3, V_4 satisfy, respectively,

$$\iint_{-\infty}^{\infty} \frac{V_1'}{R}\,\mathrm{d}\boldsymbol{x}' = 2\pi\tilde{\phi}, \tag{6.5}$$

$$\iint_{-\infty}^{\infty} \frac{V_2'}{R}\,\mathrm{d}\boldsymbol{x}' = \iint_{-\infty}^{\infty} (\eta'-\eta)\nabla'\tilde{\phi}'\cdot\nabla'\frac{1}{R}\,\mathrm{d}\boldsymbol{x}', \tag{6.6}$$

$$\iint_{-\infty}^{\infty} \frac{V_3'}{R}\,\mathrm{d}\boldsymbol{x}' = -\iint_{-\infty}^{\infty} \tilde{\phi}'[(1+D^2)^{-3/2}-1]\nabla'\cdot\left[(\eta'-\eta)\nabla'\frac{1}{R}\right]\mathrm{d}\boldsymbol{x}', \tag{6.7}$$

$$\iint_{-\infty}^{\infty} \frac{V_4'}{R}\,\mathrm{d}\boldsymbol{x}' = -\iint_{-\infty}^{\infty} \frac{V'}{R}\left[(1+D^2)^{-1/2}-1\right]\mathrm{d}\boldsymbol{x}'. \tag{6.8}$$

A Fourier transform is then applied to the equations. For the left-hand sides of (6.5)–(6.8) we obtain

$$\mathscr{F}\left\{\iint_{-\infty}^{\infty} \frac{V_j'}{R}\,\mathrm{d}\boldsymbol{x}'\right\} = \frac{2\pi}{k}\iint_{-\infty}^{\infty} V_j'\,\mathrm{e}^{-\mathrm{i}\boldsymbol{k}\cdot\boldsymbol{x}'}\,\mathrm{d}\boldsymbol{x}' = \frac{2\pi}{k}\mathscr{F}\{V_j\} \quad (j=1,\ldots,4), \tag{6.9}$$

where $\mathscr{F}$ denotes the two-dimensional Fourier transform, $k^2 = \boldsymbol{k}\cdot\boldsymbol{k}$, and where we have exploited $\mathscr{F}\{1/R\} = (2\pi/k)\mathrm{e}^{-\mathrm{i}\boldsymbol{k}\cdot\boldsymbol{x}'}$. The transformed equation (6.5) becomes $\mathscr{F}\{V_1\} = k\mathscr{F}\{\tilde{\phi}\}$, giving

$$V_1 = \mathscr{F}^{-1}\{k\mathscr{F}\{\tilde{\phi}\}\}. \tag{6.10}$$

The Fourier transform of (6.6) leads to $\mathscr{F}\{V_2\} = -k\mathscr{F}\{\eta V_1\} - \mathrm{i}\boldsymbol{k}\cdot\mathscr{F}\{\eta\nabla\tilde{\phi}\}$, giving

$$V_2 = -\mathscr{F}^{-1}\{k\mathscr{F}\{\eta V_1\}\} - \nabla\cdot(\eta\nabla\tilde{\phi}). \tag{6.11}$$

Further, from (6.7)–(6.8) we obtain

$$V_3 = \mathscr{F}^{-1}\left\{\frac{k}{2\pi}\mathscr{F}\left\{\iint_{-\infty}^{\infty} \tilde{\phi}'[1-(1+D^2)^{-3/2}]\nabla'\cdot\left[(\eta'-\eta)\nabla'\frac{1}{R}\right]\mathrm{d}\boldsymbol{x}'\right\}\right\}, \tag{6.12}$$

$$V_4 = \mathscr{F}^{-1}\left\{\frac{k}{2\pi}\mathscr{F}\left\{\iint_{-\infty}^{\infty} \frac{V'}{R}[1-(1+D^2)^{-1/2}]\,\mathrm{d}\boldsymbol{x}'\right\}\right\}. \tag{6.13}$$

We note that (the negative of) (3.1) corresponds to the one-dimensional version of $V_1 + V_2$ given in (6.10)–(6.11). The kernels of the inner integrals of (6.12) and (6.13) decay as R^{-4} and R^{-3}, respectively. As in the two-dimensional formulation, these integrals may be evaluated over a very limited region of the $\boldsymbol{x}$-plane, still keeping high accuracy. While V_1, V_2 and V_3 are determined by known functions at the free surface, V_4 is determined implicitly. The latter may be determined iteratively as in the two-dimensional case, where in the first iteration V is replaced by $V_1 + V_2 + V_3$ on the right-hand side of (6.13). The iteration procedure may then be continued until the desired accuracy is achieved. In practical computations, one iteration may be sufficient however, as found in the two-dimensional numerical examples described above.

7. Discussion

A novel fast procedure for computations of fully nonlinear non-overturning ocean surface waves is developed. The method is derived in both two and three dimensions. A corresponding computational scheme is developed in the two-dimensional case. The essential part of the method is the rapidly convergent iterative scheme whereby a solution of the Laplace equation is obtained. The number of operations required is asymptotically $O(N \log N)$. In fact, the scheme is so fast that one iteration is sufficient in practical computations, while still keeping high accuracy. This constitutes an explicit approximation of the method which is tested out in two versions, i.e. the differentiated stream functions $\tilde{\psi}_{3,x,\pi/k_0}$ and $\tilde{\psi}_{4,x,\pi/k_0}$ given by (3.2) and (3.3), respectively.

The algorithms involving $\tilde{\psi}_{3,x,\pi/k_0}$ may be put in a form where aliasing terms are avoided. Smoothing or regridding are then not required. This is particularly advantageous with regard to accurate wave simulations over long time. The simulations presented here illustrate that $\tilde{\psi}_{3,x,\pi/k_0}$ (and $\tilde{\psi}_{4,x,\pi/k_0}$) give the same results as reference computations when the wave slope $|\eta_x|$ is less than 0.35. For larger slopes, $\tilde{\psi}_{4,x,\pi/k_0}$ provides a valid description even when $|\eta_x|$ is as large as unity. The scheme involving $\tilde{\psi}_{4,x,\pi/k_0}$ is tested in a form where aliasing terms are partially avoided by extending the Fourier spectra twice. Simulations of nonlinear wave–wave interaction, carried out up to breaking, did not exhibit aliasing errors, however. No smoothing was applied.

The new schemes speed up the simulations by a large factor in the present examples as compared to the classical procedure. Both $\tilde{\psi}_{3,x,\pi/k_0}$ and $\tilde{\psi}_{4,x,\pi/k_0}$ are found to give more accurate results than the ordinary formulation when the computational grids are coarse, because their algebraic simplicity involves fewer aliasing error. These are interesting features which can be exploited in simulations of wave fields of appreciable length over long time.

The method has promising potential with regard to several important and less understood nonlinear wave phenomena. This includes the formation of freak waves, a topic that receives considerable interest from both the scientific and engineering communities. Further, fully nonlinear simulations of irregular waves including bi-directionality and short-crestedness are of relevance to the offshore industry. Another aspect is nonlinear evolution of wave groups.

For simplicity, all derivations are given for infinite water depth. The method is, however, easily extended to a fluid with constant depth, as outlined in Appendix B.1 for the two-dimensional case. Similar extension is straightforward also in three dimensions. The method may be generalized to include a variable bottom with finite slope (Appendix B.2) and to model overhanging waves (Appendix B.3).

This work was conducted under the Strategic University Programme 'General Analysis of Realistic Ocean Waves' funded by the Research Council of Norway.

Appendix A. Arbitrarily fast decaying kernels

To compute $\tilde{\psi}$ (or $\tilde{\psi}_x$), it is advantageous to first compute $\tilde{\psi}_{x^n}$ and, consequently, to obtain $\tilde{\psi}$ by integration. Numerical integrations are very fast and accurate when computed with FFT. Moreover, as integrations have a natural smoothing effect, formulae involving integrations are preferable to those involving derivatives. $\tilde{\psi}_{x^n}$ can be obtained from the generalized Cauchy integrals

$$\frac{\partial^n f}{\partial z^n} = \frac{(n-p)!}{\mathrm{i}\pi}\ \mathrm{PV}\oint_C \frac{\partial^p f'}{\partial z'^p}\frac{\mathrm{d}z'}{(z'-z)^{n-p+1}} \quad (z\in C,\ 0\leqslant p\leqslant n), \tag{A 1}$$

where $z = x + \mathrm{i}y$ and $f(z) = \phi + \mathrm{i}\psi$. Taking $p = 1$ – in order to avoid η'_x in the integral – and after multiplication by $(1+\mathrm{i}\eta_x)^n$, for infinite depth, (A 1) yields

$$(1+\mathrm{i}\eta_x)^n\partial_{\tilde{z}}^n\widetilde{f} = -\frac{(n-1)!}{\mathrm{i}\pi}\ \mathrm{PV}\int_{-\infty}^{\infty}\left(\frac{1}{x'-x}+\frac{\mathrm{i}+D}{1+D^2}\frac{\eta_x-D}{x'-x}\right)^n \tilde{f}'_x\,\mathrm{d}x', \tag{A 2}$$

with the notation $\partial_{\tilde{z}} = (1+\mathrm{i}\eta_x)^{-1}\partial_x$, $\partial_{\tilde{z}}^2 = (1+\mathrm{i}\eta_x)^{-1}\partial_x[(1+\mathrm{i}\eta_x)^{-1}\partial_x]$, etc. Equation (A 2) shows that formulae with arbitrarily fast decaying kernels can be derived. Indeed, extracting the linear part and after some integrations by parts, we obtain

$$\begin{aligned}\mathscr{H}\{\widetilde{f}_{x^n}\} = &-\mathrm{i}(1+\mathrm{i}\eta_x)^n\partial_{\tilde{z}}^n\widetilde{f}\\ &-\sum_{m=1}^{n}\frac{n!(n-1)!}{m!(n-m)!\pi}\ \mathrm{PV}\int_{-\infty}^{\infty}\left(\frac{\mathrm{i}+D}{1+D^2}\frac{\eta_x-D}{x'-x}\right)^m\frac{\tilde{f}'_x\,\mathrm{d}x'}{(x'-x)^{n-m}}.\end{aligned} \tag{A 3}$$

All the kernels of the integrals in (A 3) decay as $|x'-x|^{-n}$, but at a crest they decay faster.

The practical evaluations of the (hyper) singular integrals involved in (A 3) require the calculus derivatives of $\widetilde{f}$, but at most of order n. This is in perfect balance with the left-hand side of the equation, and hence, the equation is well-posed for numerical functional iteration.

The relation (A 3) shows that $\widetilde{f}_{x^n}$ is expressed as a function of its primitives. This is the opposite of a Taylor expansion, which expresses a function with its derivatives. Formulae like (A 3) are thus, in general, more suitable for numerical computations.

Appendix B. Generalized domains

The method outlined in § 2 is extended here to more general two-dimensional problems. All the generalizations presented here can be combined to derive further generalizations.

B.1. *Horizontal bottom*

With a horizontal bottom at $y = -h$, the Schwarz symmetry principle and the Cauchy integral yield

$$\begin{aligned}\tilde{\phi} = &\frac{1}{\pi}\int_{-\infty}^{\infty}\frac{-(x'-x)(\tilde{\psi}'+\eta'_x\tilde{\phi}')+(\eta'-\eta)(\tilde{\phi}'-\eta'_x\tilde{\psi}')}{(x'-x)^2+(\eta'-\eta)^2}\,\mathrm{d}x'\\ &-\frac{1}{\pi}\int_{-\infty}^{\infty}\frac{(x'-x)(\tilde{\psi}'+\eta'_x\tilde{\phi}')-(2h+\eta'+\eta)(\tilde{\phi}'-\eta'_x\tilde{\psi}')}{(x'-x)^2+(2h+\eta'+\eta)^2}\,\mathrm{d}x'.\end{aligned} \tag{B 1}$$

Introducing $D_\pm = (\eta' \pm \eta)/(x' - x)$, $H = 2h/(x' - x)$ and the operators

$$\mathscr{H}_\pm\{f\} = \frac{1}{\pi} \fint_{-\infty}^{\infty} \frac{f'}{x' - x}\,\mathrm{d}x' \pm \frac{1}{\pi} \int_{-\infty}^{\infty} \frac{(x' - x)f'}{(x' - x)^2 + 4h^2}\,\mathrm{d}x',$$

$$\mathscr{I}\{f\} = f - \frac{1}{\pi} \int_{-\infty}^{\infty} \frac{2hf'}{(x' - x)^2 + 4h^2}\mathrm{d}x',$$

the equation (B 1) may be rewritten along the lines of the infinite depth case, giving

$$\begin{aligned}\mathscr{H}_+\{\tilde\psi\} = &-\mathscr{I}\{\tilde\phi\} + \mathscr{H}_+\{\eta\tilde\phi_x\} - \eta\mathscr{H}_-\{\tilde\phi_x\}\\ &+\frac{1}{\pi}\int_{-\infty}^{\infty}[\arctan(D_-) - D_-]\tilde\phi'_x\,\mathrm{d}x' + \frac{1}{\pi}\int_{-\infty}^{\infty}\frac{D_-(D_- - \eta'_x)\tilde\psi'}{1 + D_-^2}\frac{\mathrm{d}x'}{x' - x}\\ &+\frac{1}{\pi}\int_{-\infty}^{\infty}\left\{\arctan\left[\frac{D_+}{1 + HD_+ + H^2}\right] - \frac{D_+}{1 + H^2}\right\}\tilde\phi'_x\,\mathrm{d}x'\\ &+\frac{1}{\pi}\int_{-\infty}^{\infty}\frac{[D_+(2H + D_+) - (1 + H^2)(H + D_+)\eta'_x]\tilde\psi'}{(1 + H^2)[1 + (H + D_+)^2]}\frac{\mathrm{d}x'}{x' - x}.\end{aligned} \tag{B 2}$$

The operators can be computed and inverted easily in the Fourier space where

$$\mathscr{F}\{\mathscr{H}_\pm\{f\}\} = \mathrm{i}\,\mathrm{sgn}(k)(1 \pm \mathrm{e}^{-2|k|h})\mathscr{F}\{f\}, \tag{B 3}$$

$$\mathscr{F}\{\mathscr{I}\{f\}\} = (1 - \mathrm{e}^{-2|k|h})\mathscr{F}\{f\}. \tag{B 4}$$

An analogous procedure can be derived with the Green function method in three dimensions.

B.2. *Variable bottom*

If we consider a non-overturning variable bottom at $y = -h - \zeta(x)$, the Cauchy integral applied at the free surface gives

$$\begin{aligned}\tilde\phi = &\frac{1}{\pi}\fint_{-\infty}^{\infty}\frac{-(x' - x)(\tilde\psi' + \eta'_x\tilde\phi') + (\eta' - \eta)(\tilde\phi' - \eta'_x\tilde\psi')}{(x' - x)^2 + (\eta' - \eta)^2}\,\mathrm{d}x'\\ &+\frac{1}{\pi}\int_{-\infty}^{\infty}\frac{(x' - x)(\bar\psi' - \zeta'_x\bar\phi') + (h + \zeta' + \eta)(\bar\phi' + \zeta'_x\bar\psi')}{(x' - x)^2 + (h + \zeta' + \eta)^2}\,\mathrm{d}x',\end{aligned} \tag{B 5}$$

where $(\bar\phi, \bar\psi)$ are the velocity potential and the stream function at the bottom. For a fixed bottom, $\bar\psi$ is an arbitrary constant, but $\bar\phi$ is unknown. An equation for $\bar\phi$ is then obtained applying the Cauchy integral at the bottom, and considering (of course) the conjugate part of the equation

$$\begin{aligned}\bar\psi = &\frac{1}{\pi}\int_{-\infty}^{\infty}\frac{(x' - x)(\tilde\phi' - \eta'_x\tilde\psi') + (h + \zeta + \eta')(\tilde\psi' + \eta'_x\tilde\phi')}{(x' - x)^2 + (h + \zeta + \eta')^2}\,\mathrm{d}x',\\ &-\frac{1}{\pi}\fint_{-\infty}^{\infty}\frac{(x' - x)(\bar\phi' + \zeta'_x\bar\psi') + (\zeta' - \zeta)(\bar\psi' - \zeta'_x\bar\phi')}{(x' - x)^2 + (\zeta' - \zeta)^2}\,\mathrm{d}x'.\end{aligned} \tag{B 6}$$

Both relations (B 5) and (B 6) can be split, without difficulty, along the lines of (2.6) and (B 2). We thus obtain a system of two coupled integrals, with fast decaying kernels, giving $\tilde\psi$.

An analogous formula can be derived if, instead of a fixed bottom, we consider a moving interface. The method can hence be generalized to stratified fluids with several homogeneous layers.

The method presented here is efficient while ζ_x is not too large, and *a fortiori* for a non-overturning bottom. For such situations, the method presented below should be preferred.

B.3. *Overturning surface*

To describe overturning waves, the use of x as an independent variable is no longer efficient. Instead, we can take the arclength coordinate s as an independent variable for a parametric description of the surface. Thus, considering x, η, $\tilde\phi$ and $\tilde\psi$ as dependent variables of s and t (implying $\mathrm{d}x = \sqrt{1-\eta_s^2}\,\mathrm{d}s$), a generalization of the Cauchy integral (2.2) can be written

$$\tilde\phi = \frac{1}{\pi}\fint_{-\infty}^{\infty} \frac{D[(1+\tilde x_s')\tilde\phi' - \eta_s'\tilde\psi'] - (1+X)[(1+\tilde x_s')\tilde\psi' + \eta_s'\tilde\phi']}{(1+X)^2+D^2}\,\frac{\mathrm{d}s'}{s'-s}, \tag{B 7}$$

where $x(s,t) = s + \tilde x(s,t)$, $D = (\eta'-\eta)/(s'-s)$, $X = (\tilde x' - \tilde x)/(s'-s)$, $\tilde\phi = \tilde\phi(s,t)$, $\tilde\phi' = \tilde\phi(s',t)$, etc. Writing the leading parts of the integral (B 7) as convolutions, we obtain

$$\begin{aligned}\mathscr{H}\{(1+\tilde x_s)\tilde\psi\} = {}& -\tilde\phi - \mathscr{H}\{\eta_s\tilde\phi\} + \mathscr{H}\partial_s\{\eta(1+\tilde x_s)\tilde\phi\} - \eta\mathscr{H}\partial_s\{(1+\tilde x_s)\tilde\phi\}\\ &+\frac{1}{\pi}\int_{-\infty}^{\infty}\frac{(X+X^2+D^2)\eta_s'\tilde\phi' - (2X+X^2+D^2)(1+\tilde x_s')\,\tilde\phi'}{(1+X)^2+D^2}\,\frac{\mathrm{d}s'}{s'-s}\\ &-\frac{1}{\pi}\int_{-\infty}^{\infty}\frac{D\eta_s'\tilde\psi' - (X+X^2+D^2)(1+\tilde x_s')\,\tilde\psi'}{(1+X)^2+D^2}\,\frac{\mathrm{d}s'}{s'-s},\end{aligned} \tag{B 8}$$

where the Hilbert transform $\mathscr{H}$ is taken with respect to s. All the regular integrals in (B 8) have kernels that decay as $|s'-s|^{-2}$. If faster decaying kernels are required, the method explained in Appendix A can be employed.

Analogous formulae can be derived with other parametric representations of the surface, such as the well-known Lagrangian description of motion. However, the corresponding relative quantity $\tilde x$ of the later (i.e. the particle displacement) is large in the presence of (local) currents. On the other hand, with variable arclength, this quantity remains relatively small. It is therefore advantageous for the efficiency of the method demonstrated in this paper.

Appendix C. Reference Cauchy integral

The classical Cauchy integral (2.3) is used as reference for numerical comparison in the paper. For comparisons with (2.6), $\tilde\psi_x$ is computed directly since its evaluation via $\tilde\psi$ is less efficient. After one differentiation with respect to x, one integration by parts and for a $2L$-periodic domain, the integral equation (2.3) becomes

$$\tilde\psi_x = \frac{1}{2L}\fint_{-L}^{L}\frac{(\tilde\phi_x' - \eta_x\tilde\psi_x')\sin\dfrac{x'-x}{L/\pi} + (\tilde\psi_x' + \eta_x\tilde\phi_x')\sinh\dfrac{\eta'-\eta}{L/\pi}}{\cosh\dfrac{\eta'-\eta}{L/\pi} - \cos\dfrac{x'-x}{L/\pi}}\,\mathrm{d}x'. \tag{C 1}$$

This integral is discretized with a constant step Δx and is evaluated via the trapezium method, which is of infinite order for periodic functions. At $x' = x$, with respect to the principal value, the discrete integrand is

$$\frac{\Delta x}{\pi}\left[\tilde\phi_{xx} + \frac{\eta_{xx}}{1+\eta_x^2}\,\frac{\tilde\psi_x - \eta_x\tilde\phi_x}{2}\right].$$

The resolution of the corresponding linear system is achieved iteratively with an SSOR algorithm.

REFERENCES

Baker, G. R., Meiron, D. I. & Orszag, S. A. 1982 Generalized vortex methods for free-surface flow problems. *J. Fluid Mech.* **123**, 477–501.

Balk, A. M. 1996 A Lagrangian for water waves. *Phys. Fluids* **8**, 416–420.

Banner, M. L. & Tian, X. 1998 On the determination of the onset of breaking for modulating surface water waves. *J. Fluid Mech.* **367**, 107–137.

Canuto, C., Haussaini, M. Y., Quarteroni, A. & Zang, T. A. 1987 Spectral Methods in Fluid Dynamics. *Springer Series in Computational Physics*. Springer.

Ceniceros, H. D. & Hou, T. Y. 1998 Convergence of a non-stiff boundary integral method for interfacial flows with surface tension. *Maths Comput*. **67**, 137–182.

Clamond, D. & Grue, J. 2000 Dynamics of the transient leading part of a wave train. *Proc. 15th Intl Workshop on Water Waves and Floating Bodies*, Caesarea, Israel (ed. T. Miloh & G. Zilman), Faculty of Engineering, Tel Aviv University, pp. 28–31.

Craig, W. & Sulem, C. 1993 Numerical simulation of gravity waves. *J. Comp. Phys.* **108**, 73–83.

Dias, F. & Kharif, C. 1999 Nonlinear gravity and capillary–gravity waves. *Ann. Rev. Fluid Mech.* **31**, 301–346.

Dold, J. W. & Peregrine, D. H. 1986 Water-wave modulation. *Proc. 20th Intl Conf. on Coastal Engineering*, American Society of Civil Engineers, Taipei, 10–14 November 1986, pp. 163–175.

Dommermuth, D. & Yue, D. K. P. 1987 A high-order spectral method for the study of nonlinear gravity waves. *J. Fluid Mech.* **184**, 267–288.

Dysthe, K. B. 1979 Note on a modification to the nonlinear Schrödinger equation for application to deep water. *Proc. R. Soc. Lond.* A **369**, 105–114.

Fenton, J. D. 1988 The numerical solution of steady water wave problems. *Comput. Geosci.* **14**, 3, 357–368.

Fenton, J. D. 1999 Numerical methods for nonlinear waves. *Advances in Coastal and Ocean Engineering*, vol. 5, pp. 241–324. World Scientific.

Fornberg, B. 1980 A numerical method for conformal mapping. *SIAM J. Sci. Stat. Comput.* **1**, 386–400.

Grue, J., Friis, A., Palm, E. & Rusås, P. O. 1997 A method for computing unsteady fully nonlinear interfacial waves. *J. Fluid Mech.* **380**, 257–252.

Hairer, E., Nørsett, S. P. & Wanner, G. 1987 Solving ordinary differential equations I. Nonstiff Problems. *Springer Series in Computational Mathematics* **8**, Springer.

ISSC 2000 Report of the Environment Committee. *14th Intl Ship and Offshore Structures Congress*, vol. 1, Nagasaki, Japan.

Longuet-Higgins, M. S. 2000 Theory of water waves derived from a Lagrangian. Part 1. Standing waves. *J. Fluid Mech.* **423**, 275–291.

Longuet-Higgins, M. S. & Cokelet E. D. 1976 The deformation of steep surface waves on water I. A numerical method of computation. *Proc. Roy. Soc. Lond.* A **350**, 1–26.

Trulsen, K. & Dysthe, K. B. 1996 Freak waves – a three-dimensional wave simulation. *Proc. 21st Symp. on Naval Hydrodynamics*, Trondheim, pp. 550–558.

Tsai, W. T. & Yue, D. K. P. 1996 Computation of nonlinear free-surface flows. *Ann. Rev. Fluid Mech.* **28**, 249–278.

Wehausen, J. V. & Laitone, E. V. 1960 Surface waves. *Handbuch der Physik*, vol. 9, pp. 446–778. Springer.

West, B. J., Brueckner, K. A., Janda, R. S., Milder, D. M. & Milton, R. L. 1987 A new numerical method for surface hydrodynamics. *J. Geophys. Res.* **92**, 11 803–11 824.

Yasuda, T. & Mori, N. 1994 High order nonlinear effects on deep-water random wave trains. *Proc. Intl Symp. Waves – Physical and Numerical Modelling*, University of British Columbia, Vancouver, Canada, pp. 823–832.